Solid-state NMR and computational investigation of solvent molecule arrangement and dynamics in isostructural solvates of droperidol

Agris Bērziņš[*,a,b] *and Paul Hodgkinson*[*,b]

[a] Faculty of Chemistry, University of Latvia, Kr. Valdemara iela 48, Riga, LV-1013, Latvia. Telephone: +(371)-67372576. E-mail: agris.berzins@lu.lv

[b] Department of Chemistry, Durham University, South Road, Durham, DH1 3LE, UK. E-mail: paul.hodgkinson@durham.ac.uk

Abstract

^{13}C, ^{15}N and ^{2}H solid-state NMR spectroscopy have been used to rationalize arrangement and dynamics of solvent molecules in a set of isostructural solvates of droperidol. The solvent molecules are determined to be dynamically disordered in the methanol and ethanol solvates, while they are ordered in the acetonitrile and nitromethane solvates. ^{2}H NMR spectra of deuterium-labelled samples allowed the characterization of the solvent molecule dynamics in the alcohol solvates and the non-stoichiometric hydrate. The likely motion of the alcohol molecules is rapid libration within a site, plus occasional exchange into an equivalent site related by the inversion symmetry, while the water molecules are more strongly disordered. DFT calculations strongly suggest that the differences in dynamics between the solvates are related to differences in the energetic penalty for reversing the orientation of a solvent molecule.

Keywords: droperidol; solid-state NMR; hydrates/solvates; isostructural solvates; solvent dynamics; spin-lattice relaxation; motional broadening; ab initio calculations

Graphical abstract

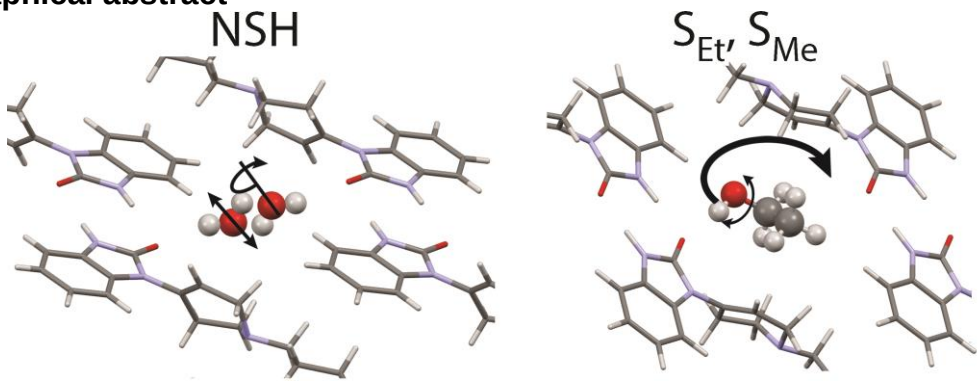

Highlights

- ^{15}N CP/MAS NMR clearly distinguishes ordered and dynamically disordered systems.
- Spectral quality is strongly correlated to ABMS broadenings.
- ^{2}H MAS NMR provides direct insight into the nature of the solvent motion.
- DFT calculations help to rationalise the differences in experimental observations.

Introduction

Solid-form screening of pharmaceutical molecules has demonstrated their propensity to adopt different forms, including polymorphs and solvates[1; 2]. It is not unusual for a pharmaceutical molecule to form more than five polymorphs[3; 4; 5] and, as reported, even in

excess of one hundred solvates[2]. Understanding and characterising these forms is essential for the pharmaceutical industry.

Solvates are typically divided in stoichiometric or non-stoichiometric solvates[6]. It is common that the same host structure can incorporate different solvent molecules to form a set of isostructural solvates. This phenomenon is typical for non-stoichiometric channel solvates [7; 8], but is not limited to non-stoichiometric solvates[9; 10; 11] nor to channel solvates[12]. The formation of isostructural solvates is typically driven by the presence of specific solvent-host interactions[9; 12] or by the specific shape of the solvent molecule [7]. It is also possible to form mixed isostructural solvates, where solvent molecules can be exchanged in only a subset of the crystallographic sites[13; 14]. Although empty host structures can be stable[15], they are typically unstable[16] or collapse immediately after the removal of the guest, despite the weak nature of the host–guest interactions[17].

Droperidol, 1-[1-[4-(4-fluorophenyl)-4-oxobutyl]-1,2,3,6-tetrahydro-4-pyridyl]-1,3-dihydro-2H-benzimidazol-2-one, Figure 1, is a neuroleptic pharmaceutical. It is reported to exist in four polymorphic forms **I** – **IV**[18; 19; 20] and eleven solvated forms[18; 19; 20; 21; 22; 23]. The solvates with methanol, ethanol, acetonitrile, nitromethane, chloroform, dichloromethane as well as the nonstoichiometric hydrate (**S_{Me}**, **S_{Et}**, **S_{ACN}**, **S_{NM}**, **S_{CLF}**, **S_{DCM}** and **NSH** respectively) are isostructural, as observed by PXRD, and crystallize in the *P*1 or *P*$\bar{1}$ space group (depending on the solvent symmetry and ordering), with two droperidol molecules in the unit cell. It has not, however, been possible to obtain diffraction quality crystals for **S_{CLF}** and **S_{DCM}** [20]. Although non-stoichiometric in that the solvent content is dependent on the partial pressure of solvent in the atmosphere – up to one equivalent of water per droperidol for **NSH**, and 0.5 equivalents of solvent for the other solvates – samples produced from crystallization are always fully solvated and are relatively stable with respect to desolvation if stored in closed containers.

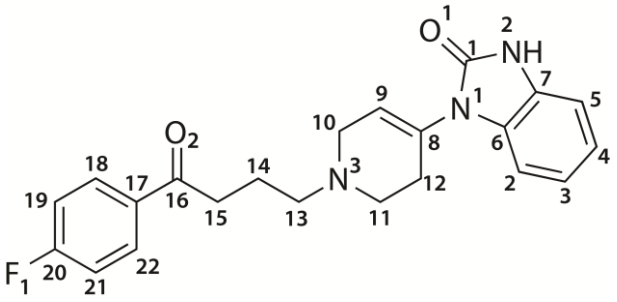

Figure 1. Molecular structure of droperidol with the numbering of non-hydrogen atoms.

Although isostructural in terms of the host droperidol structure, these solvates are unusual in that they fall into three categories. Firstly, the **NSH** crystal structure is centrosymmetric with one droperidol and one water molecule in the asymmetric unit. The water molecules occupy two nearby hydrogen-bonded positions in the channel, forming hydrogen bonds with the carboxyl group in the benzimidazolone moiety of droperidol. The isotropic displacement parameter for the water oxygen at 120 K is three times higher than for other non-hydrogen atoms, and it was not possible to locate all the water hydrogen atoms for structures determined at 173 K or above[20], suggesting that the water molecules are slightly disordered. Secondly, the **S_{Me}** and **S_{Et}** structures refine with centrosymmetry, with one droperidol and half a disordered alcohol molecule in the asymmetric unit. The alcohol molecule has the same hydrogen bond arrangement with droperidol as the water does in **NSH**. In contrast to the **NSH**, however, only one of the two droperidols in the unit cell is hydrogen bonded to the alcohol molecule, and taking into account disorder between two orientations related by inversion symmetry is necessary for a satisfactory refinement within the *P*$\bar{1}$ space group. Thirdly, the **S_{ACN}** and **S_{NM}** are non-centrosymmetric, with two droperidol and one ordered solvent molecules in the asymmetric unit, and there are no strong hydrogen bonds between the solvent and droperidol.

Solid-state NMR is now widely used in the field of pharmaceutical molecule characterization[24]. The main advantage of this method is its ability to characterize the molecular-level structure and identify possible dynamics using powdered rather than single-crystal samples[25; 26; 27; 28; 29; 30; 31]. It can be used to support or complement the information from X-ray diffraction methods[32; 33]. Although organic solvates[32; 34; 35; 36], including isostructural solvates[13; 17; 37], have been previously studied using solid-state NMR, the behaviour and dynamics of solvent molecules in isostructural solvates has not been the subject of detailed research. Typically, the NMR spectra of isostructural channel solvates are only slightly affected by changing the solvent molecules[13], as the solvent molecules introduce only minor differences in chemical environment of the host molecules, although such spectra can still be used for solvate identification[38]. Similarly, only slight changes are typically observed in NMR spectra of non-stoichiometic hydrates as function of water content[39; 40; 41], although some structural variations can be inferred[42; 43; 44].

In this study we use ^{13}C, ^{15}N and ^{2}H solid-state NMR to determine and characterize the differences between these five droperidol isostructural solvates. This includes the identification and characterization of the molecular motion in **NSH**, $\mathbf{S_{Me}}$ and $\mathbf{S_{Et}}$, to explain the slight disorder of water molecule in **NSH** and to distinguish between static vs. dynamic disorder in the alcohol solvates. Theoretical calculations are used to rationalize the differences in the molecular motion of the solvent molecules.

Experimental

Sample preparation

Droperidol (purity >99%) was obtained from JSC Grindeks (Riga, Latvia). Droperidol **NSH** was obtained by dissolving droperidol in acetone at 50 °C, adding a small amount of water and then slowly partially evaporating the resulting solution at 50 °C[20]. Droperidol solvates $\mathbf{S_{Me}}$, $\mathbf{S_{Et}}$, $\mathbf{S_{ACN}}$ and $\mathbf{S_{NM}}$ were obtained by dissolving droperidol in the corresponding solvent at 60–75 °C (depending on solvent boiling point) and then cooling the solution to –20 °C[20]. Solvates were stored in the mother liquor and filtered and dried immediately before packing into rotors.

Deuterium-labelled solvates were prepared by grinding and then desolvating the original solvate at 50 °C above P_2O_5. The resulting sample was then placed in a closed container with saturated D_2O or d_1-alcohol vapour. **NSH** with different D_2O content was obtained by storing the deuterium-labelled sample above D_2O to obtain monohydrate stoichiometry or above a saturated solution of $MgCl_2$ in D_2O to obtain approximately hemihydrate stoichiometry. These stoichiometries were estimated from previously measured sorption-desorption isotherms[20].

All of the solvents, $MgCl_2$ and P_2O_5 were purchased from commercial suppliers and used without further purification. The identity of all droperidol solvates was confirmed using PXRD[20].

Solid-state NMR

High-resolution solid-state NMR spectra were obtained using either a Bruker Avance III HD spectrometer (Bruker, Germany) operating at 125.67 MHz for ^{13}C (499.72 MHz for ^{1}H) and 76.71 MHz for ^{2}H with a 4.0 mm (rotor o.d.) MAS probe, or a Varian VNMRS 400 spectrometer (Varian Inc., USA), operating at 40.53 MHz for ^{15}N (399.88 MHz for ^{1}H) with a 6.0 mm (rotor o.d.) MAS probe. ^{15}N spectra were recorded at ambient temperature, whereas ^{13}C and ^{2}H spectra were recorded at controlled temperatures from 20 °C down to –45 °C. Note that these are set temperatures that do not attempt to correct for sample heating under magic-angle spinning; these are estimated to be of the order of +5, +8 and +15 °C for the ^{2}H, ^{15}N and ^{13}C spectra respectively.

^{13}C and ^{15}N spectra were obtained under MAS conditions using cross polarization (CP) with the following conditions: recycle delay 7–30 s for **NSH**, $\mathbf{S_{Me}}$ and $\mathbf{S_{Et}}$, and 120–180 s for $\mathbf{S_{ACN}}$,

and $\mathbf{S_{NM}}$, contact time 0.5–2 ms, a sample spin rate of 13 kHz for ^{13}C and 6.8 kHz for ^{15}N spectra, and acquiring 300–1000 transients for ^{13}C and 440–3600 transients for ^{15}N (depending on relaxation delays). SPINAL64 with 78 kHz ^{1}H nutation rate and TPPM with 55.6 kHz nutation rate were used for heteronuclear decoupling of the ^{13}C and ^{15}N spectra respectively. Spectra were referenced with respect to external neat TMS for ^{13}C or neat nitromethane for ^{15}N by setting the high-frequency signal from a replacement sample of adamantane to 38.4 ppm or the nitrate signal from a replacement sample of solid ammonium nitrate to –5.1 ppm, and typically processed with an apodisation function corresponding to a 20 Hz Lorentzian line-broadening prior to Fourier transformation. ^{13}C linewidths were determined by fitting the peaks to a mixed Lorentzian /Gaussian lineshape in the Bruker TopSpin software.

Carbon-13 T_1 values were estimated from direct-excitation spectra with recycle delays of 0.2–180 s, while more accurate measurements were made using saturation-recovery experiments with recovery delays of 0.1 ms – 90 s. 12 pulses separated with a 10 ms delay were used for saturation of the ^{13}C magnetization. 200–240 repetitions were accumulated, with a spinning rate of 13 kHz and ^{1}H decoupling nutation rate of 71 kHz. T_1 values from variable recycle delay experiments were calculated by fitting peak heights to a simple rising exponential function using Excel Solver. T_1 values from saturation-recovery experiments were determined in TopSpin by fitting integrated peak areas to a rising exponential. Note that measurement of the relaxation times for the CH_3 of $\mathbf{S_{Et}}$ in particular were complicated by transient Nuclear Overhauser effects[45]; this is discussed further in the Supplementary Information.

^{2}H MAS spectra were acquired without proton decoupling with 10 kHz spinning rate and 10 s recycle delay, acquiring 1000–10000 transients (depending on time available). T_1 relaxation times were estimated with short experiments (50–100 repetitions) with the recycle delay varying up to 10 s or 30 s using 7–9 increments. T_1 values were estimated by fitting peak heights to a simple rising exponential function as above. Bandshape analysis of the spinning sidebands was performed in Gsim[46] / pNMRsim[47] by simultaneously fitting the peak linewidths (using a Lorentzian lineshape function) and quadrupolar coupling parameters from both ND and solvent sites. Flat baselines, which are significant for fitting, were typically obtained by discarding the data points before the first rotary echo for signals obtained on-resonance. Alternatively, the baseline roll was suppressed using spline fitting in TopSpin.

First-principles computation

Chemical shift calculations were carried out using the GIPAW method implemented in CASTEP[48; 49; 50; 51], after geometry optimization of the droperidol crystal structures determined at 173 K [20]. Since the first principles calculations cannot be applied to disordered structures, starting structures of $\mathbf{S_{Me}}$ and $\mathbf{S_{Et}}$ without disorder were prepared in two ways: (a) both structures were solved in the $P1$ space group with ordered solvent and (b) $P1$ structures were derived from the reported $P\bar{1}$ structures by discarding one of the solvent molecule orientations. Calculations were performed with the PBE[52] functional using on-the-fly generated ultrasoft pseudopotentials and a cut-off energy of 600 eV, with integrals taken over the Brillouin zone using a Monkhorst-Pack grid of a minimum k-point sampling of 0.05 Å^{-1}. Two approaches were used for geometry optimization: optimization of hydrogen atom positions only and optimization of all atomic positions. Unit cell parameters were fixed to the values determined from X-ray diffraction studies in both cases. The computed ^{13}C and ^{15}N chemical shifts were referenced by linear regression of computed shielding values to the experimental shifts[50]. Geometry optimizations of doubled unit cells (see below) with adjacent solvent molecules in the same or opposing directions were performed both with the pure PBE functional and also using the Tkatchenko-Scheffler (TS) dispersion correction scheme[53]. The orientation of the solvent molecule was inverted by manually adjusting the atomic coordinates on one solvent molecule prior to full geometry optimisation.

Interaction energies between pairs of molecules were calculated in *Gaussian 09*[54] using the M06-2X[55] functional for molecular geometries directly extracted from the crystal structures

after optimization of all atom positions in CASTEP. Basis set superposition error was corrected using the counterpoise method. The pairs involved a given solvent molecule and either adjacent solvent molecules in the channels or adjacent droperidol molecules (see further discussion).

Results and discussion

Solvate characterisation using ^{13}C CPMAS spectra

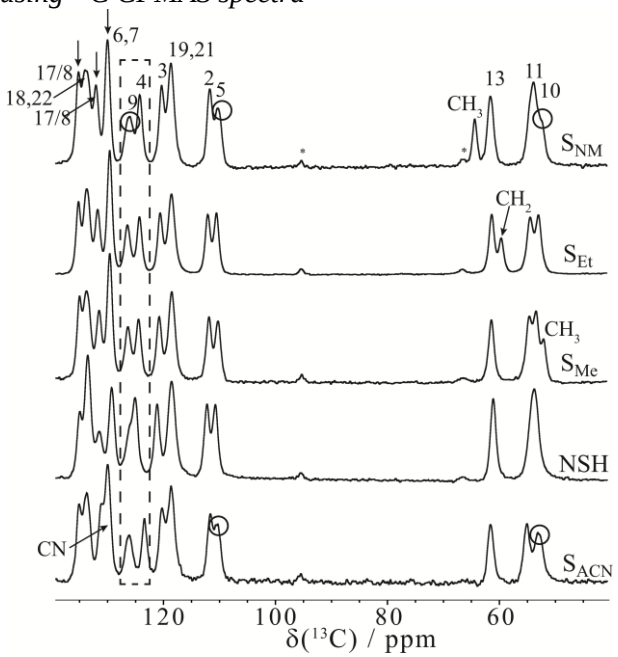

Figure 2. 50–135 ppm region of the ^{13}C CPMAS spectra of the droperidol isostructural solvates together with peak assignment. Spinning sidebands are marked with asterisks, signals absent in short CP contact time experiments are marked with arrows, and signals in the $\mathbf{S_{ACN}}$ and $\mathbf{S_{NM}}$ spectra showing evidence of splitting are circled. Full spectra are given in Figure S2.

Figure 2 shows the ^{13}C CPMAS spectra of the solvates, with the peak positions given in Table 1. The resonances of the solvent molecules are readily identified (see labels), except for the methyl group signal of ethanol and the quaternary carbon of acetonitrile, as these overlap with the peaks of droperidol. Bearing in mind that the spectra were recorded under CP conditions, and so are not strictly quantitative, the intensity of the solvent peaks is consistently around two times lower than that of the droperidol CH_2 peaks, consistent with a 0.5 solvate stoichiometry. CP spectra with short (10–50 μs) contact times were recorded (see Fig. S3) to identify the carbon atoms directly attached to hydrogen; the peaks absent in these spectra and thus associated with quaternary carbon atoms are marked with arrows in Figure 2.

As would be expected, the **NSH** spectrum is consistent with one unique droperidol molecule in the asymmetric unit. However, the $\mathbf{S_{Me}}$ and $\mathbf{S_{Et}}$ spectra also do not show clear evidence of distinct droperidol molecules in the crystal structure, one hydrogen-bonded to the solvent, and one not. Only slight splitting of some peaks, circled in Figure 2, is observed in the spectra of $\mathbf{S_{ACN}}$ and $\mathbf{S_{NM}}$, which would be consistent with having two slightly different droperidol molecules in the asymmetric unit.

To help assign the peaks, GIPAW calculations of the NMR parameters were performed for all solvates after geometry optimization. The results, after rescaling each set of the calculated shieldings against the experimental chemical shifts, are presented in Table 1. Different isotropic shielding values were calculated for the same carbon atom where inequivalent droperidol molecules are present in the asymmetric unit ($\mathbf{S_{Me}}$, $\mathbf{S_{Et}}$, $\mathbf{S_{ACN}}$ and $\mathbf{S_{NM}}$). It was observed that these differences were quite large (up to 6.8 ppm, with an average difference of 2–3 ppm, depending on the solvate) when only hydrogen atom positions were relaxed for

structures solved in the *P*1 space group. Relaxing all atomic positions during the geometry optimization decreased the average difference to 0.5 ppm. Since this is clearly in better agreement with the experimental results, only the structures obtained by all atom optimization were used in further calculations, and average values of the calculated shieldings of corresponding atoms were used when making comparisons with experimental data. The maximum difference of up to 2–3 ppm is observed for C9 and C10, which is consistent with their proximity to the solvent molecules, see Fig. S1. These results imply that solution of the XRD results in *P*1 has "exaggerated" the asymmetry between the droperidol molecules; relaxing all the atomic positions results in increased local symmetry and better agreement with the experimental NMR data.

As might be expected, the situation was reversed for the structures originally solved in $P\bar{1}$ space group ($\mathbf{S_{Me}}$ and $\mathbf{S_{Et}}$). With only optimization of the hydrogen atom positions, the droperidol environments remain essentially identical and only small maximal (1.6 to 2.2 ppm) and average (0.3 – 0.45 ppm) differences were observed for equivalent carbon shifts in the two droperidol molecules. Several of these shifts, both for solvent and droperidol sites, however, deviated significantly from the experimentally observed values. Relaxation of all atoms resulted in almost identical chemical shifts to those calculated after all-atom optimization of structures solved in *P*1.

The most significant differences between the ^{13}C spectra are observed for the C4 and C9, marked by a dashed rectangle in Figure 2; these again are close to the solvent molecules. This observation was consistent with the GIPAW calculations, where the highest difference between the average chemical shifts for different solvates were predicted to be for C9 (2.7 ppm), C4 (1.8 ppm) as well as for C8 (3.0 ppm), see Table 1. Overall, however, the spectra of solvates are very similar, showing the different solvent molecules introduce significant changes in the local chemical environment of the droperidol molecules.

Taking into account the previously identified signals from quaternary carbons and solvent atoms, the obtained shielding values after all atom optimization were plotted *versus* the observed chemical shifts, illustrated in Figure 3 for $\mathbf{S_{Et}}$. As observed previously[37; 50] and justified theoretically[56], these plots had a non-unity slope. Linear regression was used to reference the mean experimental shift to the mean computed shielding, and to rescale the calculated shifts. These plots allowed the majority of the signals to be assigned, as indicated in Figure 2, with the exceptions of strongly overlapped peaks in the region 127–135 ppm, indicated by the rectangle in Figure 3. These ambiguities are not, however, significant for the purposes of this study. Further details of the assignment are given in Table 1. In each case, a smaller RMS deviation between calculated and experimental values was observed when all atomic positions were refined, see Table 1 and Table S1.

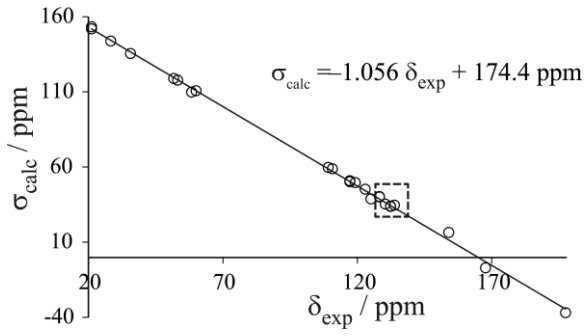

Figure 3. Calculated ^{13}C isotropic shielding (averaged over equivalent carbons) values *versus* observed chemical shifts in droperidol $\mathbf{S_{Et}}$. The dashed rectangle marks the region where the peak assignment is ambiguous.

Table 1. Assigned experimental peak maxima (in ppm) in ^{13}C CPMAS spectra and (rescaled) average calculated ^{13}C chemical shifts after all atom optimisation.

	NSH		**S_{Me}**			**S_{Et}**			**S_{ACN}**			**S_{NM}**			
Carbon	δ_{Exp}	δ_{all}	δ_{Exp}	δ_{all}	diff.[a]	δ_{Exp}	δ_{all}	diff.[a]	δ_{Exp}	δ_{all}	diff.[a]	δ_{Exp}	δ_{all}	diff.[a]	$\Delta\delta_{Calc}$[b]
C16[c]	**197.6**	199.9	**197.5**	199.9	0.1	**197.5**	199.8	0.1	**197.6**	200.2	0.2	**197.5**	199.7	0.0	0.5
C20[c,d]	**167.5**	171.5	**167.7**	171.7	0.0	**167.7**	171.6	0.1	**167.7**	171.9	0.0	**167.6**	171.6	0.0	0.4
C1[c]	**154.0**	149.2	**154.1**	149.5	0.3	**154.1**	149.3	0.1	**154.1**	149.8	0.2	**154.2**	149.7	0.4	0.6
C17/C8[c,e]	**133.6**	131.4[f]	**133.6**	131.4[g]	1.4	**133.8**	132.1[g]	0.6	**133.7**	131.4[f]	0.0	**133.9**	132.9[g]	0.8	0.1[f]
C18	**132.2**	132.7	**132.4**[h]	133.0	0.2	**132.4**	132.9	0.2	**132.3**	132.8	0.0	**132.7**[h]	133.3	0.1	0.5
C22		132.4		132.6	0.1		132.7	0.4		133.3	0.0		132.6	0.2	0.9
C17/C8[c,e]	**130.1**	130.0[g]	**130.2**	131.3[f]	0.1	**130.4**	131.4[f]	0.0	**129.8**	131.3[g]	0.2	**130.7**	131.5[f]	0.0	3.0[g]
C6[c]	**127.9**	127.1	**128.3**	127.1	0.4	**128.3**	127.0	0.4	**128.6**	127.2	0.5	**128.6**	127.4	0.2	0.4
C7[c]		126.3		126.6	0.1		126.7	0.3		127.2	0.3		127.3	0.3	1.1
C9	**124.7**	130.0	**125.0**	128.4	3.2	**125.1**	128.2	1.2	**124.8**	128.0	1.3	**124.6**[h]	127.3	2.1	2.7
C4	**123.7**	122.9	**123.1**	122.0	1.3	**123.0**	122.1	0.9	**122.1**	121.0	0.2	**122.9**	122.3	0.3	1.8
C3	**119.8**	118.1	**119.4**	118.0	0.3	**119.3**	117.9	0.3	**118.9**	117.4	0.1	**119.0**	117.5	0.0	0.6
C19	**117.2**	117.3	**117.2**	117.6	0.5	**117.3**	117.4	0.5	**117.3**	117.6	0.0	**117.3**	117.6	0.3	0.3
C21		116.5		116.7	0.0		116.7	0.4		116.8	0.0		116.8	0.0	0.4
C2[i]	**110.9**	108.7	**110.5**	108.9	0.6	**110.8**	109.2	0.6	**110.3**	108.6	0.1	**110.4**	108.8	0.2	0.6
C5[i]	**109.4**	109.0	**108.9**	107.5	1.3	**109.2**	108.3	1.1	**109.0**[h]	107.7	0.7	**108.9**[h]	107.7	0.9	1.5
C13	**59.8**	60.3	**60.1**	60.1	0.0	**60.0**	60.1	1.2	**60.3**	60.2	0.5	**60.3**	60.5	1.1	0.4
C11[i]	**52.4**	53.8	**53.3**	53.6	1.0	**53.2**	53.4	0.6	**53.7**	53.9	0.4	**52.6**[h]	53.2	1.2	0.7
C10[i]		53.2	**52.1**	53.0	0.6	**51.7**	52.3	2.1	**51.8**[h]	51.8	1.0		52.9	2.1	1.5
C15	**35.3**	36.1	**35.5**	36.1	0.0	**35.6**	36.6	0.0	**35.6**	36.5	0.0	**35.9**	37.2	0.1	1.1
C12	**28.4**	28.2	**28.4**	28.8	0.2	**28.3**	28.7	0.2	**28.0**	28.0	0.2	**28.4**	29.1	0.3	1.1
C14	**21.3**	21.0	**21.3**	21.0	0.2	**21.1**	21.1	0.0	**21.2**	20.9	0.0	**21.1**	21.2	0.0	0.3
$CH_{3\ solv}$			**50.8**	52.2		**21.1**	19.8		**4.2**	6.0		**63.1**	62.5		
CH_2/CN_{solv}						**58.3**	60.9		**128.6/ 129.8**[j]	128.3					
RMSD[k]		2.06		1.83			1.79			1.81			1.65		

[a] Difference in calculated chemical shift between two chemically equivalent atoms in the unit cell. Significant differences (greater than 0.7 ppm) are highlighted in grey (dark grey if larger than 2 ppm).

[b] Difference between the highest and lowest calculated chemical shifts from the same atom in all five solvates.

[c] Non-protonated carbons identified from short contact time CP spectrum.

[d] Signal split by J-coupling to ^{19}F, with $^{1}J_{CF}$ = 278–280 Hz in **NSH**, **S_{Me}**, **S_{Et}** and **S_{ACN}** and $^{1}J_{CF}$ = 265 Hz in **S_{NM}**.

[e] High variation in CASTEP calculated chemical shifts for these two atoms in different solvates prevents unambiguous assignment.

[f] Given value is for C17 (calculated).

[g] Given value is for C8 (calculated).

[h] Signal is slightly split.

[i] Peak separation of C2 and C5, as well as that of C10 and C11 is too small for unambiguous assignment, but consistent relative position in GIPAW calculations for all solvates (with the exception of C2 and C5 in **NSH**) and the splitting of C5 and C10 peaks support this assignment.

[j] Experimental peak position uncertain, but peak intensities and GIPAW calculations suggest that nitrile carbon corresponds to one of these peaks.

[k] Root mean square difference between experimental and calculated chemical shifts.

The experimental spectra show only slight evidence of splitting for a few peaks in $\mathbf{S_{ACN}}$ and $\mathbf{S_{NM}}$ corresponding to carbon atoms C5, C9 and C10, which are all close to the solvent molecules. The differences between peak maxima were at most 0.5 ppm, but these particular carbon atoms also show the highest splitting in the GIPAW-calculated chemical shifts, see Table 1. Observing the line splitting is complicated by the relatively broad linewidths; the widths of the peaks in the spectra of droperidol isostructural solvates were 0.75–1.15 ppm, whereas peak widths in the ^{13}C spectra of droperidol dihydrate and form **II** (see Figure S5 and S6) were only 0.32–0.70 ppm under the same conditions. This difference in linewidths can not be explained by the presence of two slightly different droperidol molecules in the unit cell, as the linewidths of the organic solvates was identical to that of **NSH**, where there is a single droperidol molecule in the asymmetric unit. The "line-broadening factors" associated with the anisotropy of the bulk magnetic susceptibility (ABMS) for powder samples[57] were determined using the magnetic susceptibility tensor calculated by CASTEP-NMR. This was found to be ~3.6 ppm for the isostructural solvates and ~1.7 ppm for both form **II** and dihydrate, suggesting that the width of the lines in the solvate spectra is associated with a large ABMS, making it intrinsically difficult to resolve overlapped resonances.

Solvate characterisation using ^{15}N CPMAS spectra

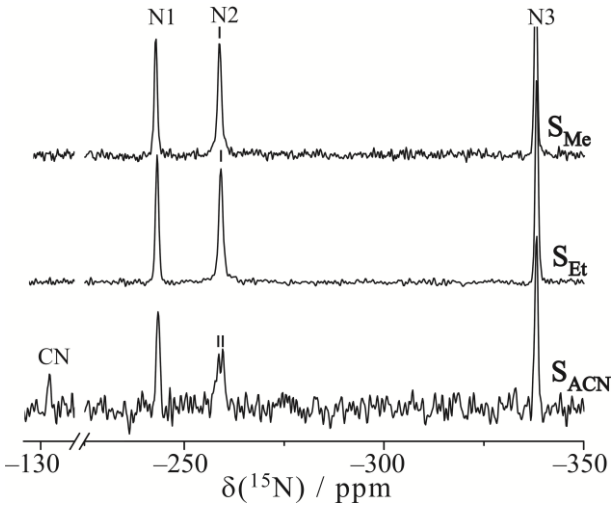

Figure 4. ^{15}N CPMAS spectra of droperidol solvates $\mathbf{S_{Et}}$, $\mathbf{S_{Me}}$ and $\mathbf{S_{ACN}}$, showing the splitting of the N2 peak in the spectrum of $\mathbf{S_{ACN}}$. The lower signal-to-noise ratio of the $\mathbf{S_{ACN}}$ spectrum reflects the much longer recycle delay needed for this sample (120 s, compared to 15 and 25 s for $\mathbf{S_{Et}}$ and $\mathbf{S_{Me}}$ respectively) and consequently a much reduced number of acquisitions compared to the alcohol solvates (440 compared to 3628 and 2308 respectively).

As shown in Figure 4, ^{15}N CPMAS spectra were recorded for the $\mathbf{S_{Et}}$, $\mathbf{S_{Me}}$ and $\mathbf{S_{ACN}}$ solvates, and peaks assigned based on the GIPAW calculations. Both $\mathbf{S_{Et}}$ and $\mathbf{S_{Me}}$ show sharp lines from all three nitrogen atoms, whereas the line from N2 – the only nitrogen atom close to the solvent – was split (or significantly broadened) in $\mathbf{S_{ACN}}$, indicating two distinct local environments. This confirms that the acetonitrile breaks the local symmetry of droperidol molecules, consistent with the determined crystal structure[20]. The experimental and GIPAW-calculated ^{15}N chemical shift differences are almost the same, 1.0 and 0.8 ppm respectively. The alcohol molecules are strongly hydrogen-bonded with the droperidol O1 atom, thus affecting the strength of the intermolecular hydrogen bond between droperidol molecules N2-H···O1 and the calculated chemical shift difference for N2 is significantly higher in $\mathbf{S_{Me}}$ and $\mathbf{S_{Et}}$, 1.6 and 3.2 ppm respectively. In contrast to $\mathbf{S_{ACN}}$, only one, somewhat broader, line is observed in the ^{15}N spectrum for the alcohol solvates (45–50 Hz for N2 compared to 35–40 Hz for other nitrogen resonances). This strongly suggests that the alcohol molecules in $\mathbf{S_{Me}}$ and $\mathbf{S_{Et}}$ are dynamically disordered, resulting in a single resonance.

Although the ^{15}N spectra were much more demanding to acquire, they are more sensitive in this case to the very subtle symmetry breaking involved. It is also worth noting in this context that ^{14}N shifts can also be very sensitive to changes in local environment as they are also dependent (via the quadrupolar 2nd order isotropic shift) on local differences in electric field gradient [58].

Characterization of solvent dynamics in droperidol isostructural solvates

The evidence from the ^{13}C and ^{15}N CPMAS spectra acquired at ambient temperature, combined with the crystal structure determinations, suggests that the solvent molecules are dynamic in $\mathbf{S_{Me}}$ and $\mathbf{S_{Et}}$. The crystal structure of **NSH** also shows evidence of disordered water molecules. ^{13}C and ^{2}H MAS spectra of $\mathbf{S_{Et}}$, $\mathbf{S_{Me}}$ and **NSH** as a function of temperature are used here to try to characterize the solvent dynamics.

Solvates with organic solvents

It can be seen in Figure 5 that the ethanol CH_2 group signal (highlighted with an arrow) in the CPMAS spectrum (solid lines) of $\mathbf{S_{Et}}$ broadens when the temperature is reduced to –15 ^{o}C and has lost most of its intensity at –40 ^{o}C. These changes are reversible and consistent with the presence of dynamics. Experiments with different contact times, see Fig. S3, confirmed that the low intensity of this peak is related to its broad nature rather than, for example, rapid $T_{1\rho}$ relaxation. The broad CH_2 peak is more easily observed in the ^{13}C direct-excitation spectra (dashed lines). The most likely mechanism for the broadening is interference between the modulation of NMR parameters by dynamics and the ^{1}H decoupling[31; 59], implying that the dynamics of the ethanol CH_2 are on the order of 10s kHz around –40 ^{o}C. It was also noticed that the build-up of the ethanol CH_2 group signal during cross-polarisation at 20 ^{o}C was significantly slower than that of CH_2 carbons of droperidol (see Fig. S8). This implies that the heteronuclear CH dipolar couplings are partially averaged by dynamics on the timescale of 10s of kHz or faster.

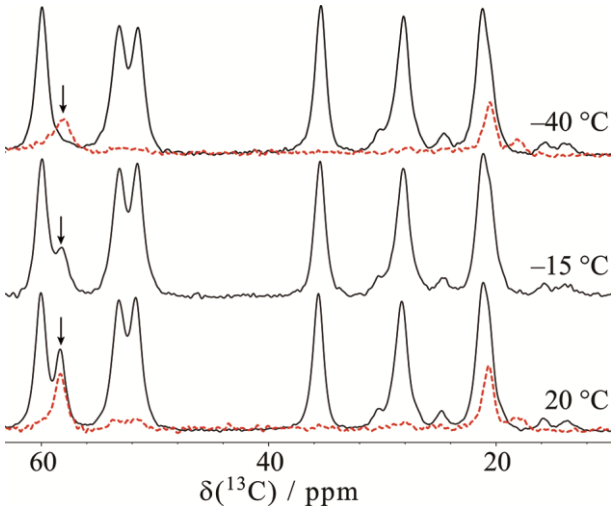

Figure 5. ^{13}C CPMAS (solid lines) and direct-excitation (dashed lines, 20 ^{o}C and –40 ^{o}C) spectra of $\mathbf{S_{Et}}$ at different temperatures. The signal from ethanol CH_2 is marked with an arrow.

The ^{13}C T_1 relaxation times measured as a function of temperature provide further insight into the dynamics of the ethanol molecules. These are tabulated in Table S2 and plotted in Figure 6. The relaxation times of both ethanol carbon atoms are relatively short e.g. 1.04 s for the CH_2 and 0.8 s for the CH_3 at 20 ^{o}C, compared to at least 50 s for the carbon atoms in droperidol. The steady decrease in T_1 relaxation time of the CH_3 carbon with decreasing temperature is consistent with the approach towards a T_1 minimum. Assuming Arrhenius-type behaviour, fitting the linear regime (i.e. excluding the data point at –40 ^{o}C) gives an activation barrier, E_a, of 15.1±0.6 kJ mol^{-1}. This is a typical value for rotational diffusion of the methyl

group[29; 30; 60], although it should be noted that a more extensive data set encompassing the T_1 minimum would provide much more robust figures. The interpretation of the CH_2 carbon data is less straightforward, but its rapid relaxation implies that there are significant local dynamics of the CH_2 over the full temperature range. While ^{13}C relaxation rates will be dominated by dipolar relaxation driven by modulations of the CH heteronuclear couplings, there will also be a contribution from cross-relaxation to any rapidly relaxing ^1H spins. Faster ^1H T_1 relaxation at lower temperatures allowed the recycle delays to be reduced from 12 s at 20 °C to 6 s at –40 °C, suggesting that the decrease in the ^{13}C T_1 of the CH_2 in the low-temperature limit may be related to faster cross-relaxation to ^1H (associated with the methyl group re-orientation). The ^{13}C T_1 of the CH_2 also decreases in the high temperature limit, where the methyl group dynamics is not contributing so effectively to T_1 relaxation. This suggests that there are additional dynamic processes that become more effective at driving the spin-lattice relaxation in the high temperature regime (and so are likely to have higher activation barrier than methyl rotation). Such processes would need to be of the order of the ^{13}C Larmor frequency (in this case 125 MHz) at 20 °C, which could also be consistent with a process that is of the order of 10s kHz at –40 °C (as observed via the spectra).

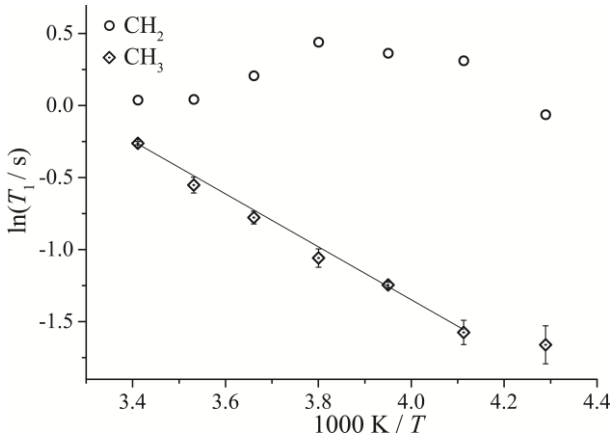

Figure 6. ^{13}C T_1 relaxation times for the ethanol carbons of $\mathbf{S_{Et}}$ as a function of inverse temperature. The one-standard-deviation error bars on the fitting of CH_2 T_1 values are of the order of the size of symbols used.

The T_1 relaxation times of methyl group carbons in methanol and acetonitrile molecules are much longer than in the ethanol solvate, 5.1 and 17 s at 20 °C respectively (see Table S2), and show the opposite temperature dependence (i.e. decreasing with increasing temperature). Bearing in mind the difficulties of interpreting relaxation data at some distance from the T_1 minimum, this suggests that the barrier for methyl group re-orientation in these solvates (and the acetonitrile solvate in particular) is significantly higher, and that the T_1 minimum is well above ambient temperature. There is also no evidence for additional high-frequency motions.

The ^2H MAS spectra of the alcohol solvates prepared from d_1-alcohols were very similar, showing resonances both from the deuterated solvent, at about 4.0 ppm, and the labile NH site of droperidol, at about 10.5 ppm. Figure 7 shows the spectra for $\mathbf{S_{Et}}$; the corresponding figure for $\mathbf{S_{Me}}$ can be found in the Supplementary Information (Fig. S10). Fitting the bandshape from both of the deuterium sites, quadrupolar coupling parameters were determined in pNMRsim[47]. The quadrupolar couplings for the ND site are uninformative, but are tabulated in Table S3. The quadrupolar coupling parameters for the alcohol OD determined from the spectra at 20 °C were found to be the same within experimental error, χ = 206 kHz, η = 0.17. The fitted quadrupolar coupling constants were slightly larger at –45 °C: χ = 211 kHz for $\mathbf{S_{Me}}$ and 222 kHz for $\mathbf{S_{Et}}$, with η = 0.17. The uncertainties on χ and η are estimated to be 2 kHz and 0.02 respectively, on the basis of duplicate measurements and different processing methods used to obtain flat spectral baselines. These parameters are consistent with values

calculated by the GIPAW calculations, χ = 244–246 kHz, η = 0.15, but reduced by high frequency motions of increasing amplitude as the temperature is increased[61]. Note that flipping of the solvent molecules through the inversion centre will not change the quadrupolar coupling tensor orientation and so would not have a direct effect on the spectrum.

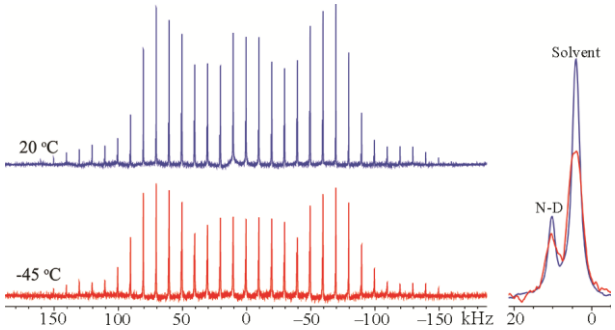

Figure 7. ^{2}H MAS spectra at a spinning rate of 10 kHz for **S_{Et}** at 20 and –45 °C, with the centreband region expanded on the right.

In contrast to the ^{2}H spectra, which might suggest that the solvent molecules are essentially static, the ^{2}H T_1 relaxation times for the alcohol OD group were short (estimated to be 0.1 – 0.3 s) at both measurement temperatures (–45 °C and 20 °C), see Table S4. Again, a simple flip of solvent molecules through an inversion centre cannot itself explain the fast relaxation, since the quadrupolar tensor is left unchanged. This implies that multiple high-frequency processes are active, resulting in fast relaxation rates that are not significantly temperature dependent, i.e. there is no single motional process creating a well-defined T_1 minimum. We have previously observed small amplitude motions that are large enough to drive relaxation but too small to significantly average the quadrupolar coupling constant[30]. The crystal structure solution and the averaged chemical environments for the droperidol molecules in the unit cell indicate that the solvent molecules are also flipping orientations, but the ^{2}H NMR data and the ^{13}C relaxation times are not sensitive to this process. The most likely scenario is that the alcohol molecules are relatively dynamic within their lattice sites and also occasionally flip over to the equivalent site related by the inversion symmetry.

Nonstoichiometric hydrate

Reduction of the temperature to –40 °C noticeably changed the ^{13}C CPMAS spectra of **NSH**, Figure 8. The largest changes are for the signals from C9 and C4, both of which are close to the water molecules – C9 is even weakly hydrogen bonded with the water[18; 20] – suggesting changes in the dynamics and/or average structure of the water molecules. The relatively short (largely temperature independent) ^{1}H T_1 relaxation time of about 15 s observed in the ^{13}C CP experiments is consistent with motion of the water molecules; droperidol phases without mobile solvent molecules, **S_{ACN}**, **S_{NM}**, polymorph **II** and dihydrate, showed T_1 values in excess of 2 min, which is more typical of molecular solids lacking methyl groups to drive relaxation.

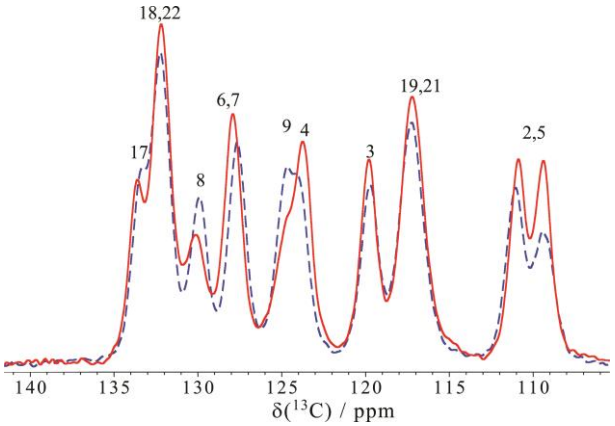

Figure 8. ^{13}C CPMAS spectra of **NSH** at 20 ^{o}C (solid line) and –40 ^{o}C (dashed line).

Figure 9 shows ^{2}H MAS spectra of **NSH** prepared from D_2O as a function of temperature. Very different bandshapes and temperature dependence are observed compared to the alcohol solvates. The water signal in **NSH** has narrower bandshape with partially averaged quadrupolar coupling parameters: χ was 84±3 kHz, while η was more variable, in the range 0.6 to 1.0, depending both on water content and temperature, see Table S3. This dependence on the water content presumably reflects changes in the overall dynamics with the degree of occupancy of water sites. While the possibility of distinct populations of static vs. dynamic water molecules can be ruled out, it is difficult to distinguish whether there is a distribution of similar water environments or a single averaged water environment with fast exchange between sites. Reducing the temperature clearly broadens the lines corresponding to D_2O, Figure 9 (b), implying the water is highly dynamic at ambient temperature and that some aspect of the dynamics is being slowed to the 10s kHz frequency scale at –45 ^{o}C. The overall quadrupolar coupling constants are somewhat lower than those typically reported for water molecules undergoing rapid C2 flips[62; 63; 64], suggesting that the overall dynamics is more complex. Moreover a simple C2 flip motion would produce η values of unity and would not explain the relatively high displacement parameters for water oxygen site observed in XRD[20]. As would be expected, the ^{2}H T_1 relaxation times for the water sites are very short, estimated to be <0.1 s from experiments with variable recycle delays. Again, the ND site is relatively uninformative; fitted quadrupolar parameters are tabulated in Table S3, T_1 relaxation times were 1–3 s (see Table S4), comparable to values observed for deuterium sites without high-frequency dynamics. The larger intensity of the ND signal in Figure 9 (a), probably reflects that the fact that the hemihydrate sample was stored for longer in the D_2O atmosphere that the monohydrate sample.

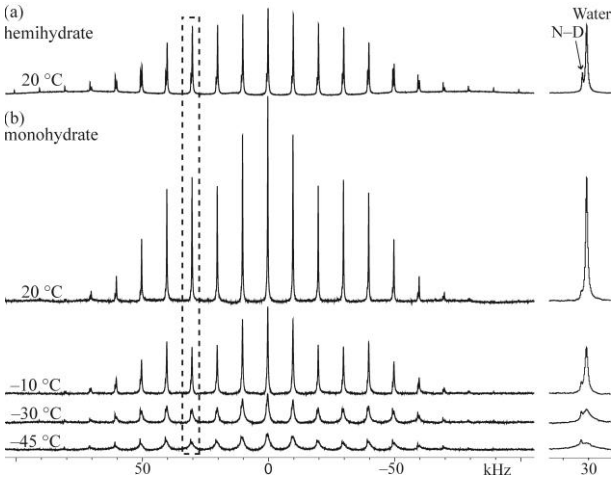

Figure 9. ^{2}H MAS spectra at a spinning rate of 10 kHz of **NSH** with (a) hemihydrate stoichiometry at 20 ^{o}C, and (b) monohydrate stoichiometry at different temperatures. The insets show the spinning sideband at about 30 kHz (marked with dashed rectangle), as the ND signal is clearer here than in the centreband. The spectra have the same vertical scale.

To quantify the motional broadening seen in Figure 9, the linewidths of the D_2O peaks (LW) were determined from the bandshape fitting of the spinning sideband manifold. The motional broadening was estimated by subtracting the width of the ND resonance (LW_o = 160 Hz), which is assumed to be unaffected by the water dynamics. The plot of linewidth due to motional broadening[65] against inverse temperature, Figure 10, is linear over this temperature range allowing an Arrhenius-type activation barrier to be determined, E_a = 25±3 kJ mol^{-1}. Note that in this fast exchange limit, the constant of proportionality between the motional broadening and the rate of dynamics is related in a non-trivial way to the quadrupolar parameters and motional mechanism. Moreover, the physical significance of the

derived activation parameter is limited given both the non-trivial nature of the motion and the restricted temperature range covered.

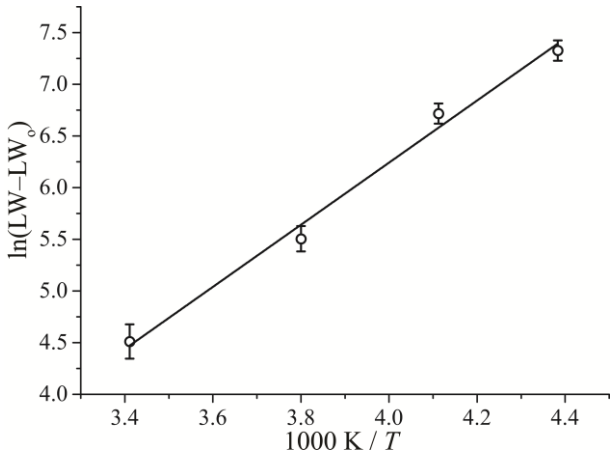

Figure 10. Estimated motional line broadening of the ^{2}H D_2O resonance of **NSH** as a function of inverse temperature. The "error bar" indicates the maximum and minimum linewidths observed using different methods for bandshape fitting / baseline roll suppression (see Experimental).

Theoretical analysis of the differences in solvent molecule behaviour

In order to rationalize the observed differences in the solvent molecule dynamics between the different droperidol solvates, the energy difference was determined between structures where all the solvent molecules in a channel point in the same direction and where adjacent solvent molecules point in opposite directions. As a first step, the orientation of the solvent molecule in each hemisolvate crystal structure was approximately reversed and geometry optimization in CASTEP used to relax all the atomic positions. The tiny energy differences of up to 0.3 kJ cell^{-1} (equivalent about 3×10^{-7} of the total cell energy) between the energies of these nominally identical unit cells gives an estimate of the "error bar" in this type of calculation. The unit cell dimensions were then doubled in the solvent channel (*a*-axis) direction and the orientation of one solvent molecule was reversed. The energy differences (per unit cell / doperidol molecule) between the "same direction" and "opposite direction" structures after full geometry optimization, with and without dispersion correction, are shown in Table 2. It can be seen that the cell energies are essentially the same for $\mathbf{S_{Et}}$, particularly when the dispersion-corrected functional is used. In contrast, the "same direction" structure is slightly energetically more favourable for $\mathbf{S_{Me}}$, and is significantly more energetically favourable for $\mathbf{S_{NM}}$ and $\mathbf{S_{ACN}}$.

Table 2. Increase in unit cell total energy (in kJ cell^{-1}) of droperidol solvates when adjacent solvent molecules are positioned in the opposite direction, with and without dispersion correction (+TS)

Solvate	$\mathbf{S_{Et}}$	$\mathbf{S_{Me}}$	$\mathbf{S_{NM}}$	$\mathbf{S_{ACN}}$
PBE	–1.5	2.9	9.9	26.3
PBE+TS	–0.4	3.7	12.6	26.9

Pairwise interaction energies were also calculated to provide insight into the energetics of different relative solvent orientations. Interaction energies (the difference in energy between two separated molecules and their dimer) were calculated using *Gaussian 09* between one solvent molecule and the two solvent and eight droperidol molecules that surround the chosen solvent molecule. The co-ordinates of these ten molecular pairs were extracted from the optimized "same direction" and "opposite direction" crystal structures, and the overall

interaction energy approximated as the sum of these ten pairwise interaction energies. In the case of the "opposite direction" structure, adjacent solvent molecules can either be oriented "head-to-head" (HH) or "tail-to-tail" (TT), see Fig. S11, along the *a*-axis direction. As required from the inversion symmetry, the total interaction energy of the solvent with its surroundings is the same, within the calculation accuracy, for the two solvent arrangements in "opposite direction" structure. As shown in Figure 11, the total interaction energy is essentially identical for the "same direction" and "opposite direction" structures in the case of **S$_{Et}$**. In contrast, the interaction energies are much more favourable for the "same direction" structure for **S$_{NM}$** and **S$_{ACN}$**. These trends are fully consistent with the pattern of total unit cell energies as observed above. As shown in Figure 11 and tabulated in Table S5, the most significant factor (at least 87%) contributing to the difference in interaction energies are the solvent-solvent interactions. The solvent-solvent interactions are always attractive in the "same direction" structure, whereas the interactions between nitromethane and acetonitrile molecules change by 13–18 kJ mol^{-1} from attractive to repulsive in the "opposite direction" structure.

These results provide a straightforward rationalisation of the absence of solvent disorder in the **S$_{ACN}$** and **S$_{NM}$** solvates – where there is a strong energetic preference for the solvent molecules to be consistently oriented – and the presence of solvent molecule disorder in **S$_{Me}$** and **S$_{Et}$**, where there is little energetic preference for a consistent orientation.

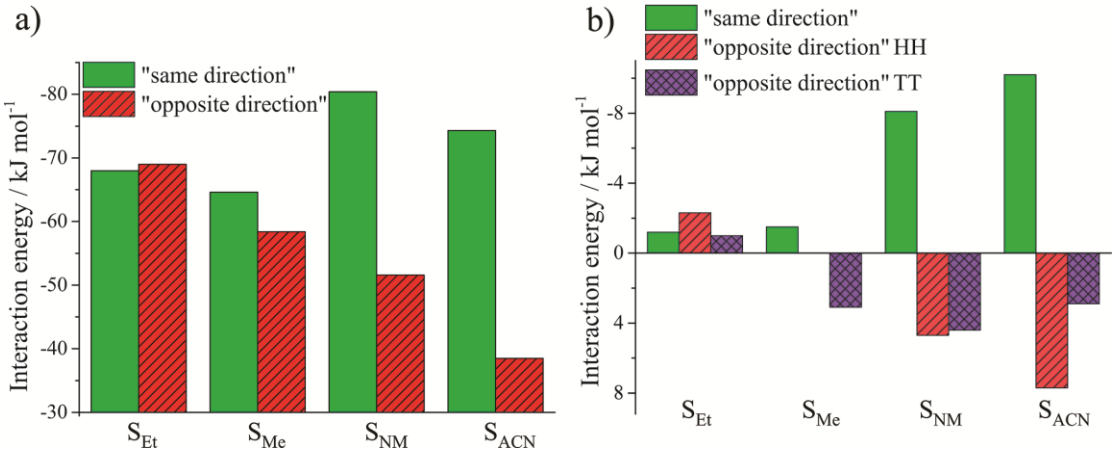

Figure 11. Calculated (a) total pair-wise interaction energies of solvent molecules and (b) solvent-solvent interaction energies, in "same direction" and "opposite direction" droperidol solvate structures.

Conclusions

The ^{13}C CPMAS solid-state NMR spectra of a set of isostructural solvates of droperidol (**NSH**, **S$_{Me}$**, **S$_{Et}$**, **S$_{ACN}$** and **S$_{NM}$**) confirm that the solvent molecules have only minor effect on the chemical environment of the droperidol molecules. The relatively broad linewidths, which make it difficult to resolve the inequivalence of the droperidol molecules in the **S$_{ACN}$** and **S$_{NM}$** solvates, can be explained by high anisotropy of the bulk magnetic susceptibility. The nature of the disorder was somewhat easier to resolve in the ^{15}N CPMAS spectra, where dynamic disorder in the **S$_{Me}$** and **S$_{Et}$** results a single sharp set of peak for the droperidol nitrogen sites.

Variable-temperature ^{13}C and ^{2}H spectra and measurements of spin-lattice relaxation times allow the characterization of the solvent molecule dynamics in **NSH**, **S$_{Me}$** and **S$_{Et}$**. The motion of the alcohol molecules in **S$_{Me}$** and **S$_{Et}$** contains dynamics of relatively high-frequency (on the order of 10s MHz to drive ^{2}H and ^{13}C T_1 relaxation), but of limited amplitude (given the minimal averaging of the ^{2}H quadrupolar parameters). The absence of well-defined T_1 minima suggests that this is a complex motion. The dynamics also includes components on the 10s kHz frequency scale (observed via the ^{13}C spectra) and allows for occasional flipping

over to the equivalent state related by the inversion symmetry, although the rate of this process cannot be estimated with any precision; the ^{15}N spectra set a lower limit of about 40 Hz at ambient temperature (corresponding to collapsing a frequency difference of about 1 ppm at 40.53 MHz ^{15}N Larmor frequency). The motion of the water molecules in **NSH** is also expected to be a composite motion, resulting in greater averaging of the NMR parameters than a simple C2 flip between equivalent positions, with an estimated C2 flip rate on the order of 10s kHz in –45 °C temperature, although an Arrhenius-type activation barrier of E_a = 25±3 kJ mol^{-1} could be estimated in this case.

The computational simulations help to rationalise these observations. There is little energy difference between initial and final states for inverting the orientation of the alcohol molecule in the $\mathbf{S_{Me}}$ and $\mathbf{S_{Et}}$ solvates. Although the barrier to inversion may be relatively high, this means that the solvent molecules appear to be disordered between the two symmetry-equivalent positions over the timescale of the XRD and NMR experiments. In contrast, the unfavourable energetics associated with adjacent acetonitrile and nitromethane molecules having opposite directions means that the $\mathbf{S_{ACN}}$ and $\mathbf{S_{NM}}$ are strongly ordered on the NMR and XRD timescales. These unfavourable energetics are mostly associated with solvent-solvent interaction energies.

Acknowledgments

This work was supported by the European Social Fund within the project "Support for Doctoral Studies at the University of Latvia". We thank David C. Apperley and A. Fraser Markwell for recording ^{15}N CPMAS spectra and assistance.

References

[1] C.P. Price, G.D. Glick, and A.J. Matzger, Dissecting the Behavior of a Promiscuous Solvate Former. Angew. Chem., Int. Ed. 45 (2006) 2062-2066.

[2] A.L. Bingham, D.S. Hughes, M.B. Hursthouse, R.W. Lancaster, S. Tavener, and T.L. Threlfall, Over one hundred solvates of sulfathiazole. Chem. Commun. (2001) 603-604.

[3] L. Yu, G.A. Stephenson, C.A. Mitchell, C.A. Bunnell, S.V. Snorek, J.J. Bowyer, T.B. Borchardt, J.G. Stowell, and S.R. Byrn, Thermochemistry and Conformational Polymorphism of a Hexamorphic Crystal System. J. Am. Chem. Soc. 122 (2000) 585-591.

[4] D.E. Braun, T. Gelbrich, V. Kahlenberg, R. Tessadri, J. Wieser, and U.J. Griesser, Conformational polymorphism in aripiprazole: Preparation, stability and structure of five modifications. J. Pharm. Sci. 98 (2009) 2010-2026.

[5] J.B. Nanubolu, B. Sridhar, V.S.P. Babu, B. Jagadeesh, and K. Ravikumar, Sixth polymorph of aripiprazole - an antipsychotic drug. CrystEngComm 14 (2012) 4677-4685.

[6] U.J. Griesser, The Importance of Solvates. in: R. Hilfiker, (Ed.), Polymorphism in the Pharmaceutical Industry, WILEY-VCH Verlag GmbH & Co. KGaA, Weinheim, 2006, pp. 211-233.

[7] T. Hosokawa, S. Datta, A.R. Sheth, N.R. Brooks, V.G. Young Jr, and D.J.W. Grant, Isostructurality among five solvates of phenylbutazone. Cryst. Growth Des. 4 (2004) 1195-1201.

[8] R. Banerjee, P.M. Bhatt, and G.R. Desiraju, Solvates of Sildenafil Saccharinate. A New Host Material. Cryst. Growth Des. 6 (2006) 1468-1478.

[9] N. Stieger, W. Liebenberg, J. Wessels, H. Samsodien, and M. Caira, Channel inclusion of primary alcohols in isostructural solvates of the antiretroviral nevirapine: an X-ray and thermal analysis study. Struct. Chem. 21 (2010) 771-777.

[10] N. Schultheiss, J.P. Smit, and J.A. Hanko, Three isostructural solvates of finasteride and their solid-state characterization. Eur. J. Pharm. Sci. 38 (2009) 498-503.

[11] D.E. Braun, T. Gelbrich, V. Kahlenberg, R. Tessadri, J. Wieser, and U.J. Griesser, Stability of Solvates and Packing Systematics of Nine Crystal Forms of the Antipsychotic Drug Aripiprazole. Cryst. Growth Des. 9 (2009) 1054-1065.
[12] M.R. Caira, G. Bettinetti, and M. Sorrenti, Structural relationships, thermal properties, and physicochemical characterization of anhydrous and solvated crystalline forms of tetroxoprim. J. Pharm. Sci. 91 (2002) 467-481.
[13] A. Othman, J.S.O. Evans, I.R. Evans, R.K. Harris, and P. Hodgkinson, Structural study of polymorphs and solvates of finasteride. J. Pharm. Sci. 96 (2007) 1380-1397.
[14] H. Mimura, S. Kitamura, T. Kitagawa, and S. Kohda, Characterization of the non-stoichiometric and isomorphic hydration and solvation in FK041 clathrate. Colloids Surf., B 26 (2002) 397-406.
[15] B.J. Murphy, M.J. Casteel, B. Samas, and J.F. Krzyzaniak, Thermodynamic stability considerations for isostructural dehydrates. J. Pharm. Sci. 101 (2012) 1486-1495.
[16] G. Stephenson, E. Groleau, R. Kleemann, W. Xu, and D. Rigsbee, Formation of isomorphic desolvates: Creating a molecular vacuum. J. Pharm. Sci. 87 (1998) 536-542.
[17] S. Byard, A. Abraham, P.J.T. Boulton, R.K. Harris, and P. Hodgkinson, A multi-technique approach to the study of structural stability and desolvation of two unusual channel hydrate solvates of finasteride. J. Pharm. Sci. 101 (2012) 176-186.
[18] A. Actins, R. Arajs, S. Belakovs, L. Orola, and M. Veidis, The Crystal and Molecular Structure of a Polymorph and a Pseudo-Polymorph of Droperidol. J. Chem. Crystallogr. 38 (2008) 169-174.
[19] M. Azibi, M. Draguet-Brughmas, and R. Bouche, Polymorphisme des butyrophenones: benperidol et droperidol. Pharm. Acta Helv. 57 (1982) 182-188.
[20] A. Bērziņš, E. Skarbulis, T. Rekis, and A. Actiņš, On the formation of droperidol solvates: characterization of structure and properties. Cryst. Growth Des. 14 (2014) 2654-2664.
[21] N.M. Blaton, O.M. Peeters, and C.J. De Ranter, 1-{1-[4-(4-Fluorophenyl)-4-oxobutyl]-1,2,3,6-tetrahydro-4-pyridyl}-1,3-dihydro-2H-benzimidazol-2-one dihydrate (Dehydrobenzperidol®). Acta Crystallogr., Sect. B 36 (1980) 2828-2830.
[22] L. Orola, Synthesis, structure and properties of crystalline forms of some active pharmaceutical ingredients, Ph.D. thesis, Riga Technical University, Riga, 2010.
[23] C.L. Klein, J. Welch, and L.C. Southall, Structure of droperidol–ethanol (1/1). Acta Crystallogr., Sect. C 45 (1989) 650-653.
[24] F.G. Vogt, Evolution of solid-state NMR in pharmaceutical analysis. Future Med. Chem. 2 (2010) 915-921.
[25] M. Geppi, G. Mollica, S. Borsacchi, and C.A. Veracini, Solid-State NMR Studies of Pharmaceutical Systems. Appl. Spectrosc. Rev. 43 (2008) 202-302.
[26] R.K. Harris, Applications of solid-state NMR to pharmaceutical polymorphism and related matters. J. Pharm. Pharmacol. 59 (2007) 225-239.
[27] R.K. Harris, NMR studies of organic polymorphs & solvates. Analyst 131 (2006) 351-373.
[28] P.A. Tishmack, D.E. Bugay, and S.R. Byrn, Solid-state nuclear magnetic resonance spectroscopy—pharmaceutical applications. J. Pharm. Sci. 92 (2003) 441-474.
[29] E. Carignani, S. Borsacchi, and M. Geppi, Dynamics by Solid-State NMR: Detailed Study of Ibuprofen Na Salt and Comparison with Ibuprofen. J. Phys. Chem. A 115 (2011) 8783-8790.
[30] D.C. Apperley, A.F. Markwell, I. Frantsuzov, A.J. Ilott, R.K. Harris, and P. Hodgkinson, NMR characterisation of dynamics in solvates and desolvates of formoterol fumarate. Phys. Chem. Chem. Phys. 15 (2013) 6422-6430.
[31] P. Hodgkinson, Intramolecular Motion in Crystalline Organic Solids. in: R.K. Harris, R.E. Wasylishen, and M.J. Duer, (Eds.), NMR Crystallography, Wiley, 2009.
[32] F.G. Vogt, D.E. Cohen, J.D. Bowman, G.P. Spoors, G.E. Zuber, G.A. Trescher, P.C. Dell'Orco, L.M. Katrincic, C.W. Debrosse, and R. Curtis Haltiwanger, Structural

analysis of polymorphism and solvation in tranilast. J. Pharm. Sci. 94 (2005) 651-665.
[33] F.G. Vogt, R.C.B. Copley, R.L. Mueller, G.P. Spoors, T.N. Cacchio, R.A. Carlton, L.M. Katrincic, J.M. Kennady, S. Parsons, and O.V. Chetina, Isomorphism, Disorder, and Hydration in the Crystal Structures of Racemic and Single-Enantiomer Carvedilol Phosphate. Cryst. Growth Des. 10 (2010) 2713-2733.
[34] R.K. Harris, P.Y. Ghi, H. Puschmann, D.C. Apperley, U.J. Griesser, R.B. Hammond, C. Ma, K.J. Roberts, G.J. Pearce, J.R. Yates, and C.J. Pickard, Structural Studies of the Polymorphs of Carbamazepine, Its Dihydrate, and Two Solvates. Org. Process Res. Dev. 9 (2005) 902-910.
[35] J. Ruiz, V. Rodriguez, N. Cutillas, A. Hoffmann, A.-C. Chamayou, K. Kazmierczak, and C. Janiak, Structure-solid-state CPMAS 13C NMR correlation in palladacycle solvates (pseudo-polymorphs) with a transformation from $Z' = 1$ to $Z' = 2$. CrystEngComm 10 (2008) 1928-1938.
[36] R.K. Harris, P. Hodgkinson, T. Larsson, A. Muruganantham, I. Ymén, D.S. Yufit, and V. Zorin, Characterization of Polymorphs and Solvates of Terbutaline Sulfate. Cryst. Growth Des. 8 (2008) 80-90.
[37] D.C. Apperley, A.F. Markwell, R.K. Harris, and P. Hodgkinson, NMR characterisation of structure in solvates and polymorphs of formoterol fumarate. Magn. Reson. Chem. 50 (2012) 680-690.
[38] G.A. Stephenson, J.G. Stowell, P.H. Toma, D.E. Dorman, J.R. Greene, and S.R. Byrn, Solid-State Analysis of Polymorphic, Isomorphic, and Solvated Forms of Dirithromycin. J. Am. Chem. Soc. 116 (1994) 5766-5773.
[39] F.G. Vogt, P.C. Dell'Orco, A.M. Diederich, Q. Su, J.L. Wood, G.E. Zuber, L.M. Katrincic, R.L. Mueller, D.J. Busby, and C.W. DeBrosse, A study of variable hydration states in topotecan hydrochloride. J. Pharm. Biomed. Anal. 40 (2006) 1080-1088.
[40] R.L. Te, U.J. Griesser, K.R. Morris, S.R. Byrn, and J.G. Stowell, X-ray Diffraction and Solid-State NMR Investigation of the Single-Crystal to Single-Crystal Dehydration of Thiamine Hydrochloride Monohydrate. Cryst. Growth Des. 3 (2003) 997-1004.
[41] P. Chakravarty, R.T. Berendt, E.J. Munson, V.G. Young, R. Govindarajan, and R. Suryanarayanan, Insights into the dehydration behavior of thiamine hydrochloride (Vitamin B1) hydrates: Part I. J. Pharm. Sci. 99 (2010) 816-827.
[42] F. Kang, F.G. Vogt, J. Brum, R. Forcino, R.C.B. Copley, G. Williams, and R. Carlton, Effect of Particle Size and Morphology on the Dehydration Mechanism of a Non-Stoichiometric Hydrate. Cryst. Growth Des. 12 (2011) 60-74.
[43] S.M. Reutzel, and V.A. Russell, Origins of the unusual hygroscopicity observed in LY297802 tartrate. J. Pharm. Sci. 87 (1998) 1568-1571.
[44] D.C. Apperley, P.A. Basford, C.I. Dallman, R.K. Harris, M. Kinns, P.V. Marshall, and A.G. Swanson, Nuclear magnetic resonance investigation of the interaction of water vapor with sildenafil citrate in the solid state. J. Pharm. Sci. 94 (2005) 516-523.
[45] A. Findlay, and R.K. Harris, Measurement of nuclear overhauser enhancements in polymeric films. J. Magn. Reson. 87 (1990) 605-609.
[46] V. Zorin, Gsim – a visualisation and processing program for solid-state NMR, URL: http://gsim.sourceforge.net, 2013.
[47] P. Hodgkinson, pNMRsim: a general simulation program for large problems in solid-state NMR, URL: http://www.dur.ac.uk/paul.hodgkinson/pNMRsim, 2013.
[48] C.J. Pickard, and F. Mauri, All-electron magnetic response with pseudopotentials: NMR chemical shifts. Phys. Rev. B 63 (2001) 245101.
[49] S.J. Clark, M.D. Segall, C.J. Pickard, P.J. Hasnip, M.I. Probert, K. Refson, and M.C. Payne, First principles methods using CASTEP. Z. Kristallogr. 220 (2005) 567-570.
[50] R.K. Harris, P. Hodgkinson, C.J. Pickard, J.R. Yates, and V. Zorin, Chemical shift computations on a crystallographic basis: some reflections and comments. Magn. Reson. Chem. 45 (2007) S174-S186.

[51] J.R. Yates, C.J. Pickard, and F. Mauri, Calculation of NMR chemical shifts for extended systems using ultrasoft pseudopotentials. Phys. Rev. B 76 (2007) 024401.
[52] J.P. Perdew, K. Burke, and M. Ernzerhof, Generalized Gradient Approximation Made Simple. Phys. Rev. Lett. 77 (1996) 3865-3868.
[53] A. Tkatchenko, and M. Scheffler, Accurate Molecular Van Der Waals Interactions from Ground-State Electron Density and Free-Atom Reference Data. Phys. Rev. Lett. 102 (2009) 073005.
[54] M.J. Frisch, G.W. Trucks, H.B. Schlegel, G.E. Scuseria, M.A. Robb, J.R. Cheeseman, G. Scalmani, V. Barone, B. Mennucci, G.A. Petersson, H. Nakatsuji, M. Caricato, X. Li, H.P. Hratchian, A.F. Izmaylov, J. Bloino, G. Zheng, J.L. Sonnenberg, M. Hada, M. Ehara, K. Toyota, R. Fukuda, J. Hasegawa, M. Ishida, T. Nakajima, Y. Honda, O. Kitao, H. Nakai, T. Vreven, J.A.J. Montgomery, J.E. Peralta, F. Ogliaro, M. Bearpark, J.J. Heyd, E. Brothers, K.N. Kudin, V.N. Staroverov, R. Kobayashi, J. Normand, K. Raghavachari, A. Rendell, J.C. Burant, S.S. Iyengar, J. Tomasi, M. Cossi, N. Rega, J.M. Millam, M. Klene, J.E. Knox, J.B. Cross, V. Bakken, C. Adamo, J. Jaramillo, R. Gomperts, R.E. Stratmann, O. Yazyev, A.J. Austin, R. Cammi, C. Pomelli, J.W. Ochterski, R.L. Martin, K. Morokuma, V.G. Zakrzewski, G.A. Voth, P. Salvador, J.J. Dannenberg, S. Dapprich, A.D. Daniels, O. Farkas, J.B. Foresman, J.V. Ortiz, J. Cioslowski, and D.J. Fox, Gaussian 09, Gaussian Inc., Wallingford, CT, 2009.
[55] Y. Zhao, and D. Truhlar, The M06 suite of density functionals for main group thermochemistry, thermochemical kinetics, noncovalent interactions, excited states, and transition elements: two new functionals and systematic testing of four M06-class functionals and 12 other functionals. Theor. Chem. Acc. 120 (2008) 215-241.
[56] M. Dračínský, and P. Hodgkinson, Effects of Quantum Nuclear Delocalisation on NMR Parameters from Path Integral Molecular Dynamics. Chem. Eur. J. 20 (2014) 2201-2207.
[57] A.J. Robbins, W.T.K. Ng, D. Jochym, T.W. Keal, S.J. Clark, D.J. Tozer, and P. Hodgkinson, Combining insights from solid-state NMR and first principles calculation: applications to the 19F NMR of octafluoronaphthalene. Phys. Chem. Chem. Phys. 9 (2007) 2389-2396.
[58] A.S. Tatton, T.N. Pham, F.G. Vogt, D. Iuga, A.J. Edwards, and S.P. Brown, Probing Hydrogen Bonding in Cocrystals and Amorphous Dispersions Using 14N–1H HMQC Solid-State NMR. Mol. Pharm. 10 (2013) 999-1007.
[59] W.P. Rothwell, and J.S. Waugh, Transverse relaxation of dipolar coupled spin systems under rf irradiation: Detecting motions in solids. J. Chem. Phys. 74 (1981) 2721-2732.
[60] A.J. Horsewill, Quantum tunnelling aspects of methyl group rotation studied by NMR. Prog. Nucl. Magn. Reson. Spectrosc. 35 (1999) 359-389.
[61] M. Dracinsky, and P. Hodgkinson, A molecular dynamics study of the effects of fast molecular motions on solid-state NMR parameters. CrystEngComm 15 (2013) 8705-8712.
[62] R.R. Vold, Deuterium NMR studies of dynamics in solids and liquid crystals. in: R. Tycko, (Ed.), Nuclear Magnetic Resonance Probes of Molecular Dynamics, 1994, pp. 27-112.
[63] G. Soda, and T. Chiba, Deuteron Magnetic Resonance Study of Cupric Sulfate Pentahydrate. J. Chem. Phys. 50 (1969) 439-455.
[64] T. Chiba, and G. Soda, Deuteron Quadrupole Interactions in Two Modifications of Oxalic Acid Dihydrate Crystal. Bull. Chem. Soc. Jpn. 44 (1971) 1703-1704.
[65] N.H.M. Hogg, P.J.T. Boulton, V.E. Zorin, R.K. Harris, and P. Hodgkinson, Use of rotary echoes in magic-angle spinning NMR for the quantitative study of molecular dynamics. Chem. Phys. Lett. 475 (2009) 58-63.